ORIGINAL ARTICLE

lajss.org
Latin American Journal of Solids and Structures

www.lajss.org

Numerical and experimental investigation of the ballistic performance of the armor structure with in-layer deflector against bullets

Mehmet Çalışkan[a]*, Erdal Camcı[b], Fehim Findik[c,d]

[a] Mechanical Engineering Department, Sakarya University of Applied Sciences, Serdivan, Sakarya. E-mail: caliskan@subu.edu.tr
[b] Arifiye Vocational School, Sakarya University of Applied Sciences, Arifiye, Sakarya, Turkey. E-mail: erdalc@subu.edu.tr
[c] Metallurgical and Materials Engineering Department, Sakarya University of Applied Sciences, Serdivan, Sakarya.
[d] BIOENAMS R&D Group, Sakarya University, Sakarya, Turkey. E-mail: findik@subu.edu.tr

* Corresponding author

https://doi.org/10.1590/1679-78257269

Abstract

This is a study to investigate ballistics performance of armor structures with in-layer deflector against projectiles. For this purpose, the armor structure, which consists of a v-cross section sheet metal array covered with aluminum and steel plates, has been designed and optimized. Firstly, numerical simulations were studied using the finite-element method (FEM). The ANSYS LS-DYNA FE software is used for the ballistic analysis. The Johnson-Cook constitutive equation and damage model were used to model the behavior of metal armors under impact in the ballistic simulations. In the next step, experimental studies were carried out. Penetration depths were measured; including the magnitude of plate bending in front of the target plate and bulging behind it. Comparisons between the results of the finite element analysis (FEA) and the tests reveal that a bullet with a velocity of 868 m/s penetrated the target, but the target could not be penetrated at a firing speed of 631 m/s Furthermore the experimental and numerical results were in good agreement.

Keywords

Ballistic, impact, armor, finite element analysis, failure analysis, steel, aluminum.

Graphical Abstract

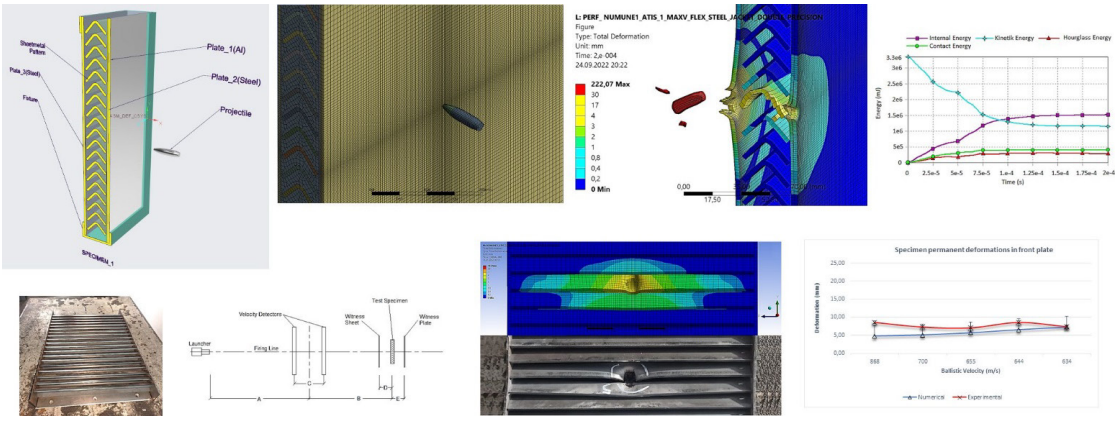

Received: September 03, 2022. In revised form: October 11, 2022. Accepted: November 8, 2022. Available online: November 9, 2022
https://doi.org/10.1590/1679-78257269

1 INTRODUCTION

The idea of placing deflectors between layers of armor to protect soldiers on battlefields is often neglected due to the long manufacturing time. A review of the literature reveals that current studies generally focus on layered systems and deflector designs used for protection from bomb explosions and landmines. For example, Shou-hong and Zhen-hua (2011) investigated deflector plate designs for the protection of truck cabins from explosions. Hafizi et al. (2017) experimentally and numerically investigated the behavior of a V-shaped deflector design against bomb explosions. Clayton (2015) numerically investigated the ballistic behavior of a composite sheet consisting of ceramic-polymer-metal layers. Behera et al. (2021) investigated the explosion protection performance of a V-shaped composite plate design. Kang et al. (2021) investigated the performance of V-shaped armor plates against land mines through experimental and numerical studies. Panowicz et al. (2013) numerically investigated the mine protection performance of metal sheet designs with deflector geometry for placement on the underside of armored vehicles. In their study, Fernández et al. (2011) numerically investigated a ceramic armor model in order to minimize the material fracture damage caused by bullet impacts and to lighten the weight. Roth et al. (2020) investigated the usability of Al7020 as a light armor material experimentally and numerically with the temperature-dependent perforation parameter. Wang et al. (2013) carried out experimental and numerical studies for a hybrid composite armor design. Doherty et al. (2012) conducted research on the usability of aluminum alloy plates for light armor protection. Grujicic et al. (2007) conducted research on the ballistic performance of alumina reinforced polymer matrix composite armors against armor-piercing bullets. Going further back, it is understood that Wilkins (1977) conducted research on the design of light armor with Boron additives. As a result of these studies, it is understood that studies focused on both layered and deflected ballistic performance have not been done sufficiently.Therefore, this study aims to investigate the ballistic performance of a lightened version of layered armor with deflectors.

2 METHODS AND MATERIALS

2.1 Finite Element Method

The development of armor systems is costly as it requires extensive research processes. Penetration and puncture scenarios involve different damage mechanisms and are complex. In addition, the physical conditions in impact zones can change with temperature, strain rate, stress, and pressure (Crouch 2017). This approach is inadequate as it only considers the effects of hydrostatic pressure in ballistics. This has led to the development of hydrocode software that allows the definition of deviatoric stress components. The calculation of the energy, mass, and momentum conservation equations is the basis of all hydrocodes in the ballistic penetration analysis. This process is realized in the form of dimension and time decompositions using the finite element method (FEM). In dynamic processes where large and sudden deformations occur, such as in terminal ballistic and explosion modeling, small time interval integration should be used to observe the wave propagation in micro- and nanoseconds and to improve the non-linearity of these glitches (Crouch 2017 and Zukas 2004). This study used the finite element analysis (FEA) software ANSYS LS-DYNA, which has been shown by many studies to be suitable for ballistic analysis. LS-DYNA used for the non-linear analysis of structures subjected to large deformations, especially with a small time interval method. It uses different contact-effect algorithms that allow for the analysis of contact problems that are difficult to solve, such as element deletion with ballistic effects. It is necessary to use data cards suitable for analysis to ensure the effective use of this software, which has a large library of material models and different contact algorithm types. The Lagrangian method used in the FEA in the current investigation is based on the partitioning of continuous materials to resolve the dynamic stress wave propagation observed in ballistic simulations (Crouch 2017). The rigid body is separated into N elements and has a mesh structure. In Lagrangian calculations, the material is entrenched in the mesh. Thus, the displacement, rotation, and distortion of the network structure can represent the material behavior. As the density of the network structure increases, the accuracy of the calculations increases; however, this can cause a sharp increase in the computation time. Therefore, the most suitable network structure should be selected to achieve negligible deviations in the results. The most suitable network structure is the one in which the deviations in the solutions are negligible and the computation time is shortest. For the damage estimation of the shot plates, the elements were concentrated in the area in contact with the bullet, and the dimensions of the elements were reduced from 1 mm to 0.25 mm. Similar analyses previously reported in the literature have indicated that it is sufficient to use 0.25 × 0.25 × 0 × 25 mm3 elements in regions where the number of elements is large, such as for metals (Flores-Johnson et al. 2011 and Borvik et al. 2009). Figure 1 shows the CAD model representing the 1st sample – 1st shooting experiment (CREO® 8. 2021). The CAD model is parametric. It was modelled using the PTC CREO program.

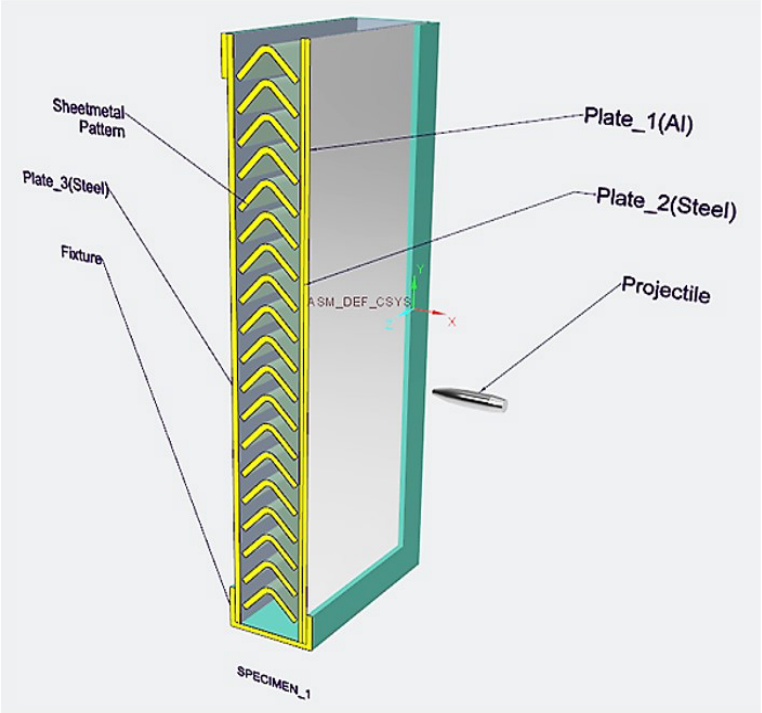

Figure 1 CAD model of the armor system designed using CREO Parametric software.

The "Bonded" contact mechanism available in the LS-DYNA FE program was used to define the combined structure of the test sample. No gaps remained between the parts, and the friction coefficient was neglected. For the contact between the bullet core and the plates, the “Contact_Eroding_Surface_To_Surface” contact mechanism available in the program was deemed appropriate, and the “Hourglass” control option was used to prevent hourglass-shaped misdirection of deformation.

In ballistic simulations, the Johnson-Cook (J-C) constitutive equation and damage model, which have been proven by many studies in the literature, were used to model the behavior of metal armors under impact. The J-C strength model is used to determine the yield stress from experiments performed at different strain rates and temperatures. It can describe the stress–strain relationships of metal materials under high deformation, high strain rate, and high-temperature conditions (Johnson and Cook 1983).

$$\sigma_{eş} = f(\varepsilon_{eş}, \dot{\varepsilon}_{eş}^{\,*}, T) \tag{1}$$

$$\sigma_{eş} = (A + B.\varepsilon_{eş}^{\,n})(1 + C.\ln \dot{\varepsilon}_{eş}^{\,*})(1 - T^{*m}) \tag{2}$$

Where, $\varepsilon_{eş}$ is the deformation, and A, B, and n are material constants with hardening. $\dot{\varepsilon}_{eş}{}^{*}$ defines strain hardening with a constant C. T refers to the thermal softening arising from the adiabatic temperature increase with a constant m. The J-C model is obtained by multiplying the three cases mentioned above. The first pair of parentheses in Equation 2 considers the increase in the yield stress due to hardening. The shear stress required to produce continuous shear in the metal increases continuously with an increase in the unit strain. Hardening results from the relationship between the dislocations and the obstacles that prevent their movement within the crystal structures in the material. The second pair of parentheses represents the increase in the yield strength with increasing strain rate. ε is a dimensionless parameter and is represented by Equation 3.

$$\dot{\varepsilon}_{eş}^{\,*} = \frac{\dot{\varepsilon}_{eş}}{\dot{\varepsilon}_0} \tag{3}$$

Where, $\dot{\varepsilon}_0$ is the reference unit strain rate defined by the user. The last parentheses in Equation 2 represent the homologous temperature $T*$. This temperature-dependent term reveals the thermal unstiffening of the substance due

to the thermal-plastic imbalance. This term is defined as the ratio of the yield stress at an increased temperature to the yield stress at ambient temperature.

$$T^* = \frac{(T - T_o)}{(T_e - T_o)} \tag{4}$$

Here, the subscript "o" refers to 20°C, and the sub-index "e" indicates the melting temperature; the temperature rise is assumed to occur adiabatically. The temperature rise due to adiabatic warming was calculated using the following equation:

$$\Delta T = \int_0^{\dot{\varepsilon}_{eş}} x \frac{\sigma_{eş}.d.\varepsilon_{eş}}{\rho.c_p} \tag{5}$$

Where, ρ is the material density, Cp is the specific heat, and x is the Taylor-Quinney coefficient representing the rate of plastic deformation work transformed into heat. For steels, the Taylor-Quinney coefficient is 0.9 (Borvik et al. 2009). The Johnson-Cook strength model was then evolved into a model in which the effects of stress triaxiality, temperature, strain rate, and strain on damage were defined (Johnson and Cook 1985).

$$D = \sum \frac{\Delta\varepsilon_{eş}}{\varepsilon_f} \tag{6}$$

Here, $\Delta\varepsilon_{eş}$ denotes the increment of the equivalent plastic unit deformation that occurs during an integration cycle. ε_f is the unit strain for fracture under certain strain rate, temperature, and equivalent stress conditions. D is a function of five different damage parameters and occurs when the fracture state is D = 1. In other words, $\sum \Delta\varepsilon_{eş} = \varepsilon_f$ for breaking to occur. In the original J-C model, the second pair of parentheses, which denotes the sensitivity to the unit strain rate, was modified to avoid undesirable effects when $\dot{\varepsilon}_{eş}$<1.

$$\sigma_{eş} = (A + B.\varepsilon_{eş}^{\ n})(1 + \dot{\varepsilon}_{eş}^{\ *})^c (1 - T^{*m}) \tag{7}$$

In this study, to observe the damage effects, it was deemed appropriate to use the modified J-C (MJC) material model given in Equation 7. Furthermore, temperature-based damage was defined in the simulations to determine the JC damage parameters. Johnson-Cook damage parameters for fracture strain are given in Equation 8.

$$\varepsilon_f = (D_1 + D_2 \exp(D_3\sigma^*))(1 + D_4 \ln(\dot{\varepsilon}_{eş}^*))(1 + D_5 T^*) \tag{8}$$

The effects of the three parentheses on the fracture strain can be expressed as the stress triaxiality effect, the strain rate effect and the temperature effect, respectively. D_1, D_2, D_3, D_4 and D_5 represent the d obtained from the tests and $\sigma^* = \bar{\sigma} / \sigma_{eş}$ stress triaxiality. In the stress triaxiality equation, the hydrostatic stress is expressed by the expression $\bar{\sigma}$. The critical temperature value is taken as $T_{kr} = 0.9T_e$ (Borvik et al. 2009), which indicates that the elements will be erased if the temperature reaches 90% of the melting point. It is assumed that when the critical temperature is reached, the strength of the material becomes too low and the material cannot resist impact. The values of the material models used in the model are given in tables 1 and 2 (Dehgolan et al. 2016 and Öztürk 2010).

Table 1. Properties for J-C material model

Material	Strength Parameters				
	A (MPa)	B (MPa)	n	C	m
St 37	200	250	0.36	0.022	1
Al 2024 T351	265	426	0.34	0.015	1
Bullet	1539	477	0.18	0.012	1

Table 2. Properties for J-C material model

Material	Damage Parameters				
	D_1	D_2	D_3	D_4	D_5
St 37	0.05	3.44	-2.12	0.002	0.61
Al 2024 T351	0.05	5	-3	0.003	0.85
Bullet	0	0	0	0	0

The J-C parameters used in this study for St 37 steel were obtained from previous experimental studies (Dehgolan et al. 2016). The J-C parameters used for Al2024 and bullet materials are available in the ANSYS engineering data source explicit materials library. The bullet (100Cr6) material represents the standard 7.62 × 51 mm armor piercing core cartridge material.

The definitions of the strength parameters in Table 1 are as follows: A = yield stress, B = hardening constant, n = hardening exponent, C = strain rate constant, m = thermal softening exponent. In addition, the definitions of the damage parameters in Table 2.

The mechanical properties of the St37 target materials were examined and found to be quite close to those of AISI 1006 steel with a yield strength of 285 MPa. Considering this similarity, the AISI 1006 damage parameters were used to represent St37. Many different damage parameter values have been obtained for Al2024 T351 in many experimental studies. Considering that the relative effect of this material is less than that of steel, damage parameters close to that of St37 were chosen to represent aluminum. Figure 2 shows the relationship between the stress and strain for Al 2024 T351, St 37 steel, and bullet (100 Cr 6).

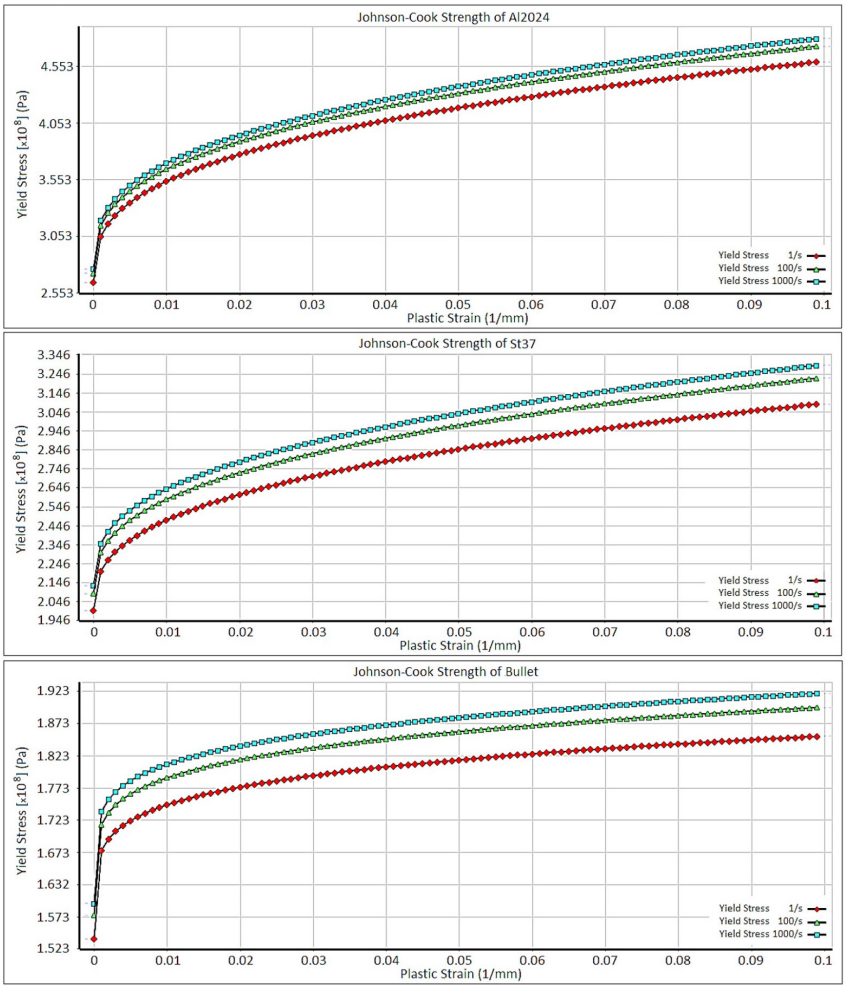

Figure 2 Stress (σ)-strain (ε) relationship for Al 2024 T351, St37 steel, and bullet (100 Cr 6) in J-C models.

Damage includes deformation beyond the design limits. If metals are subjected to stresses beyond the yield limit, they undergo permanent plastic deformation. The definition of the yield stress is sufficient for one-dimensional (1D) strain, but different yield criteria are required for more complex stress situations. Plastic deformation is studied macroscopically by deformation, microscopically by shear boundaries, and atomically by dislocation movement. The stress-strain condition can sometimes result in fracture, which is expressed by the separation of atomic bonds, as in this study.

During the deformation of ductile materials, a contraction zone occurs in the cross section. As a result, the microvoids in the narrowed cross-section are coalesced under shear and hydrostatic stresses, and the material is slowly damaged. Adiabatic shear, which is mostly observed in armors, occurs when the thermal softening speed exceeds the hardening speed when the bullet penetrates the target, and it occurs especially at high unit strain rates (Hazel 2016). If an experiment is performed under adiabatic conditions, where heat flow is inhibited, the temperature of the sample increases, resulting in thermal softening with a decrease in the hardening rate. A low thermal conductivity and a small deformation time (high velocity) are required for the occurrence of adiabatic slip. Therefore, adiabatic shear is specific to impact loading. The deformation of metals owing to the impact of blunt drill bits is caused by adiabatic shear. This deformation can also be observed under the influence of pointed bullets, as shown in this study (İbiş 2021). As shown in Figure 2, the stress-strain curve exhibited an elastic (linear) behavior during the initial period and then increased with an increase in the plastic strain for the Al, steel, and bullet specimens. It can also be observed that the stress showed a maximum value (1539 MPa) in the bullet and a minimum value at St 37 (200 MPa). In addition, higher stress values are obtained at a higher strain rate (1000/s) compared to lower strain rates, namely 100/s and 1/s, owing to the strain hardening in the case of increasing deformation speed.

2.2 FE model and firing test setup

In the first stage, 215 × 300 mm different V-shaped steel sheet and aluminum 2024 T351 sheets were modeled separately and meshed in Ansys/LS-Dyna. Modeling the wear of the bullet and taking measurements of composite plates are beyond the scope of this research, primarily because they are already well known in the literature. The focus of this work is to create a V-shaped sheet steel pattern with a backing plate. A model suitable for the geometry of the deformable 7.62x51 NATO bullet was used to represent the bullet. Quadratic tetrahedral elements were used for all bodies and the model was challenged using a fixed structure at the outer edges of the plates, as suggested in previous studies (Garcia-Avila et al. 2015, Fountzoulas-La Salvia 2012 and Garcia-Avila et al. 2014). The bullet and armor material properties used in this study are as follows: 7.62x51 mm NATO standard bullet [7.62mm diameter and 51mm long full metal jacket]. Aluminum sheets and V-shaped bent steel (2, 3 and 4mm thick). A total of 16 simulations were tried until the stability of the model was verified in the study. It was decided to choose 2 full models as deformable-damageable and rigid bullet core. With these models, a total of 4 final simulations were performed at ballistic upper and lower limit velocities. In Figure 3, the finite element model used in the study is shown. The mesh quality diagram of the FE model is shown in Figure 4. This criteria provides a composite quality metric that ranges between 0 and 1. This metric is based on the ratio of the volume to the sum of the square of the edge lengths for 2D quad/tri elements or the square root of the cube of the sum of the edge lengths for 3D elements. A value of 1 indicates a perfect cube or square while a value of 0 indicates that the element has zero or negative volume. Intensive mesh has been used in the contact areas of the model to keep the element quality high and to prevent the hourglass effect.

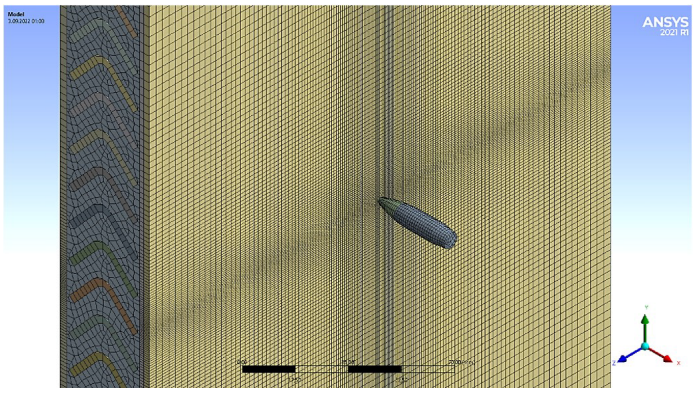

Figure 3 FE model made using a three-dimensional explicit elements (contains 90403 elements and 186961 nodes).

The real prototypes of the armor model prepared by FE analysis were manufactured as test samples. In Figure 5, one of the test specimens manufactured and the finished version mounted on the fixture is seen. The real shot test setup

is shown in Figure 6. The test was performed with 7.62 mm x 51 FJ/PB/SC ammunition. The dimensions are as follows: A: 7.5 meters, B: 2.5 meters, C: 2 meters, D=E: 0,5 meters. The launcher on the test rig is actually a foundation mounted on a Heckler Koch G3 assault rifle, and the target shots were fired with this standard NATO rifle.

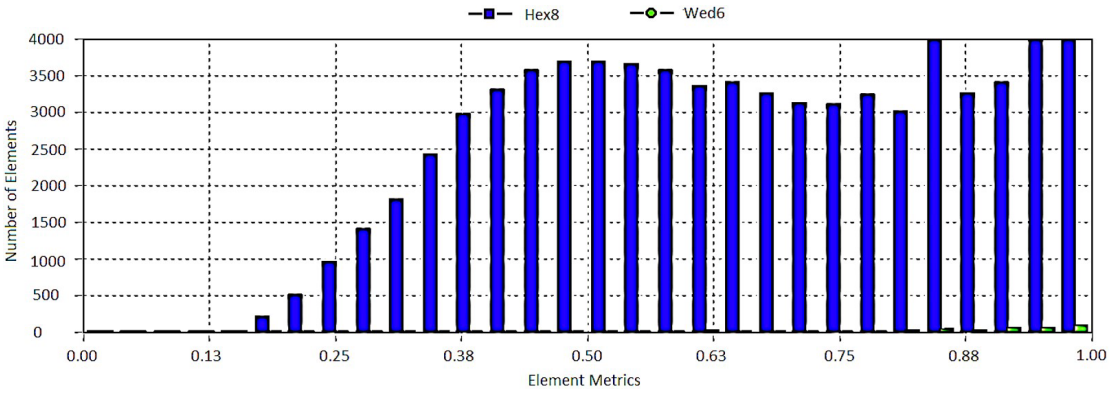

Figure 4 Mesh quality of FE model.

Figure 5 Test specimen

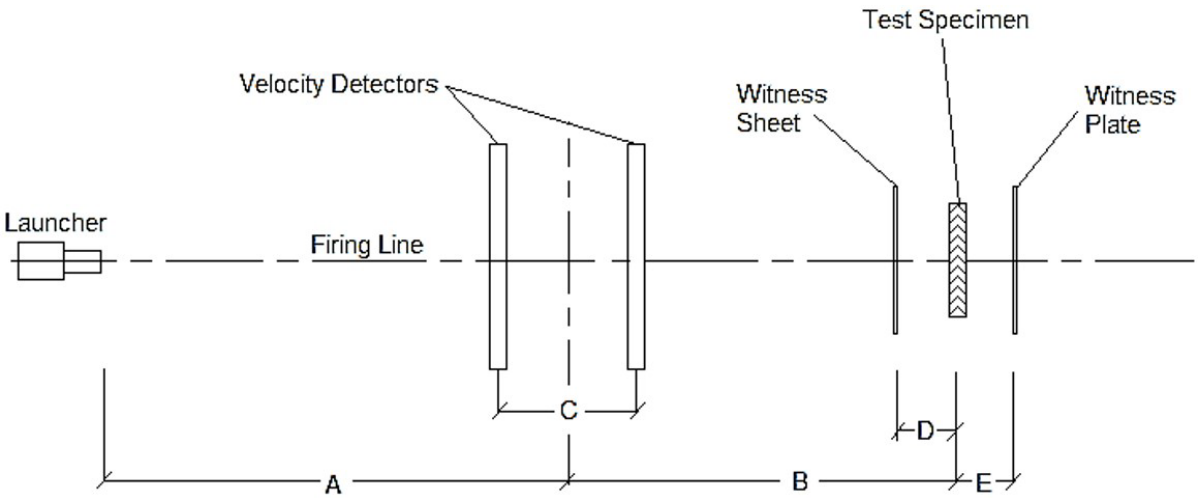

Figure 6 The shot test setup.

3 RESULTS AND DISCUSSION

3.1 FEM Results

In this study, until the stability of the model was verified, a total of 16 simulations were performed, and two full models, i.e., deformable-damageable bullet core were selected. Using these models, four final simulations were

performed at the ballistic upper and lower limit velocities obtained from the experimental results.However, some points deserve attention and will be discussed in this section. These points will be separated in short topics, as follows. Figures 7 and 8 show the energy summary and time increment of the ballistic simulation at the limit velocity (868 m/s). It is observed that the energy changes are logical and the total energy is conserved, and it is understood that the solution is convergent.

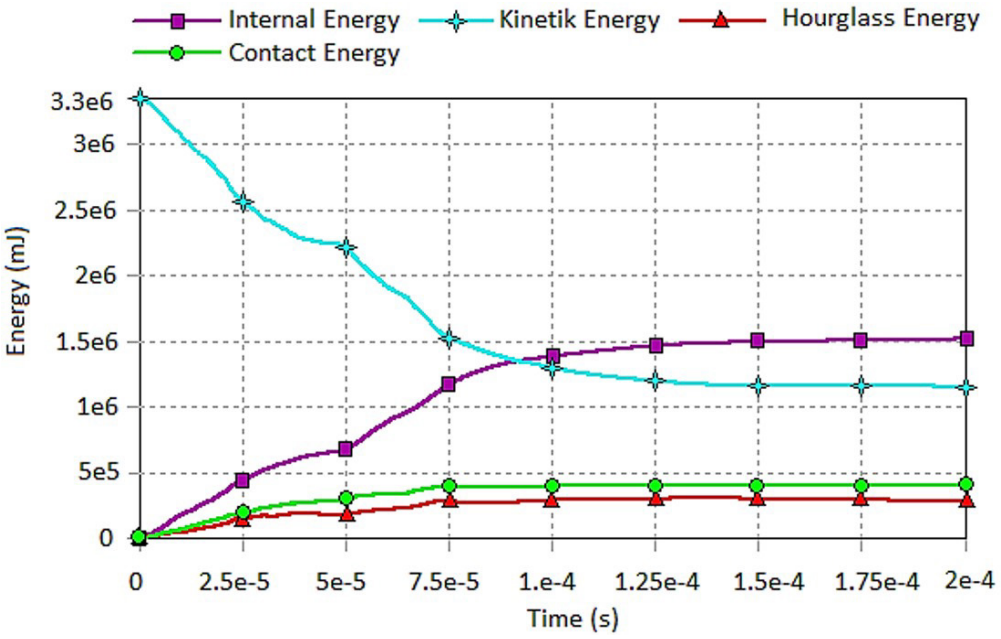

Figure 7 Energy summary of simulation with ballistics above the limit velocity (868 m/s).

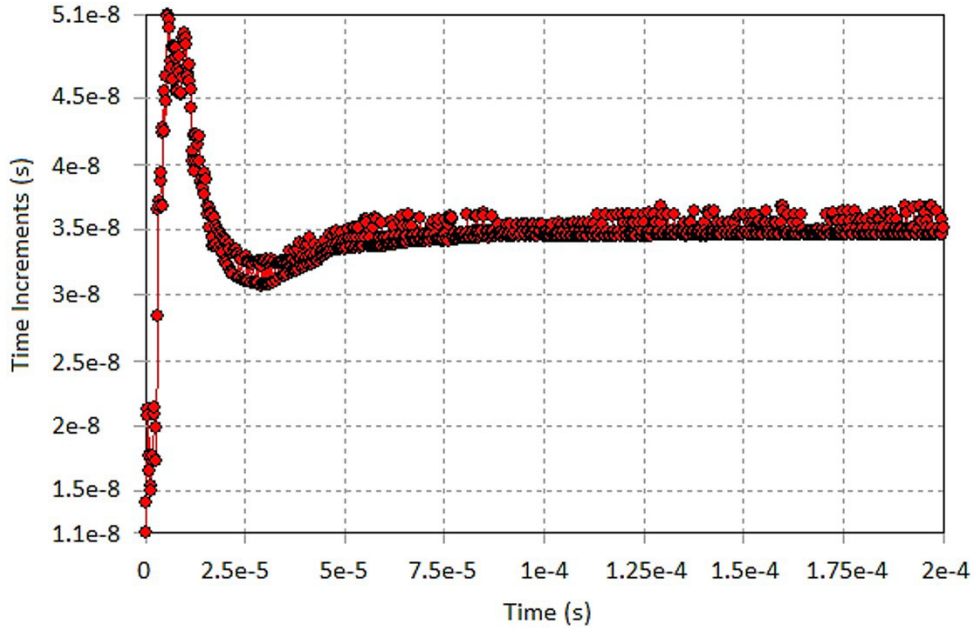

Figure 8 Time increment of simulation with ballistics above the limit velocity (868 m/s).

The results of the analyzes performed at the ballistic upper and lower limits are shown in figures 9-16.

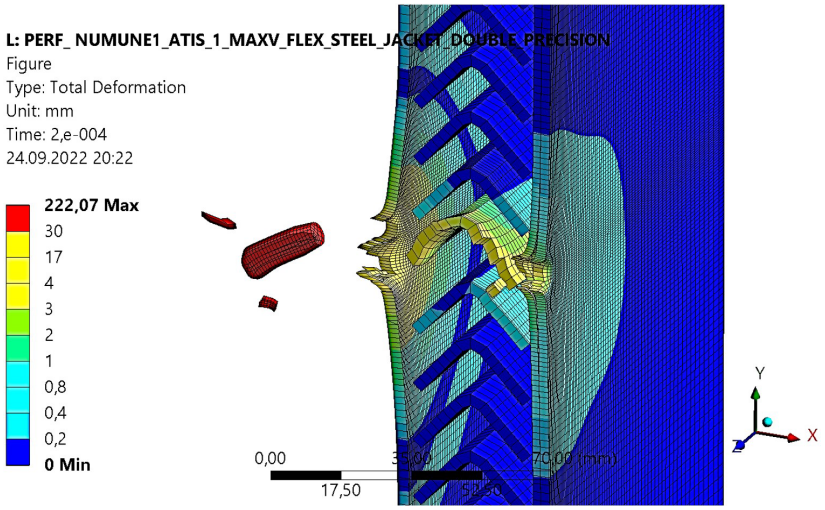

Figure 9 Deformation results of simulation with ballistics above the limit velocity (Shot 1: 868 m/s) in sectional view.

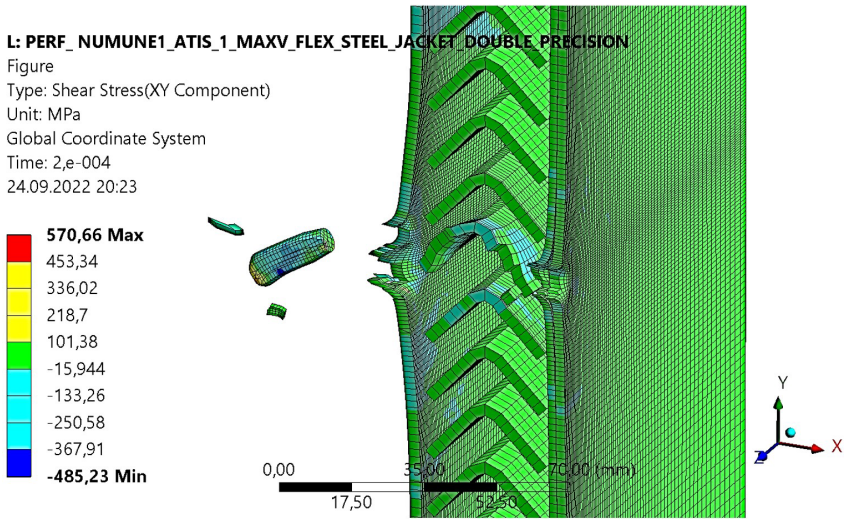

Figure 10 Shear stress distribution for Shot 1 in sectional view.

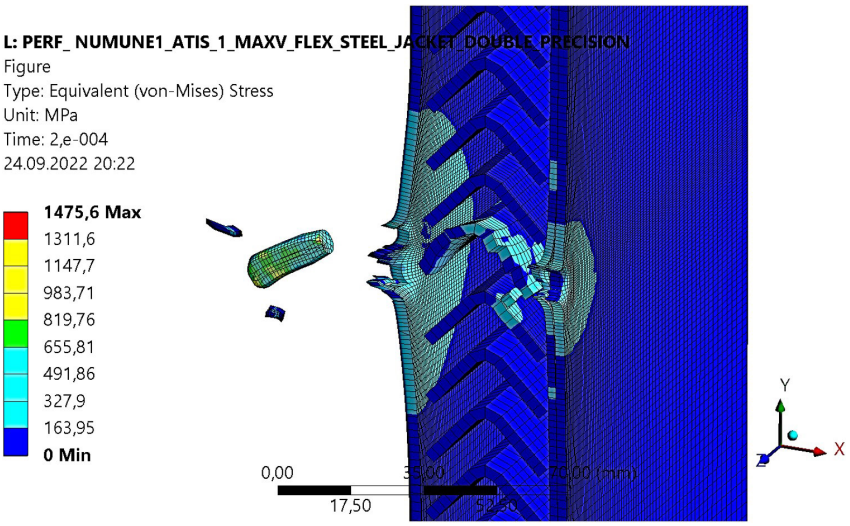

Figure 11 Von Mises equivalent stress distribution for Shot 1 in sectional view.

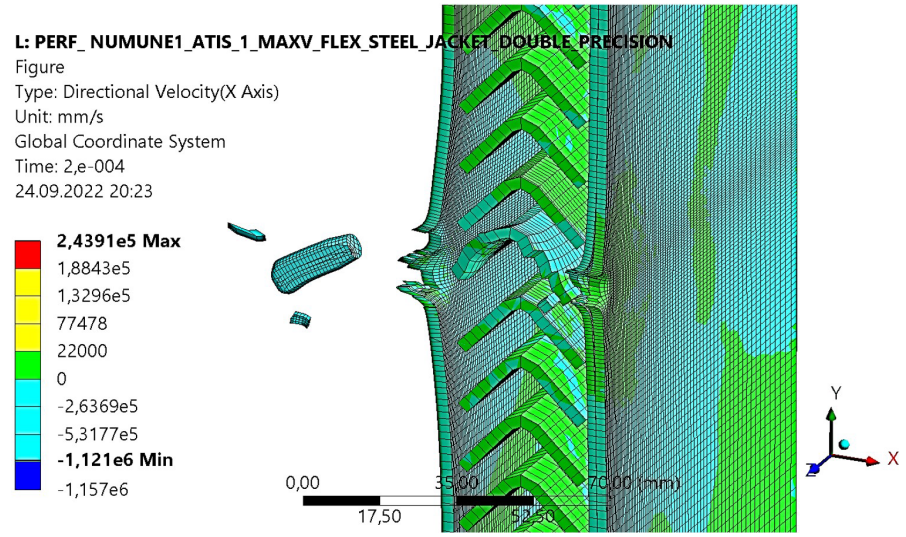

Figure 12 Velocity distribution for Shot 1 in sectional view.

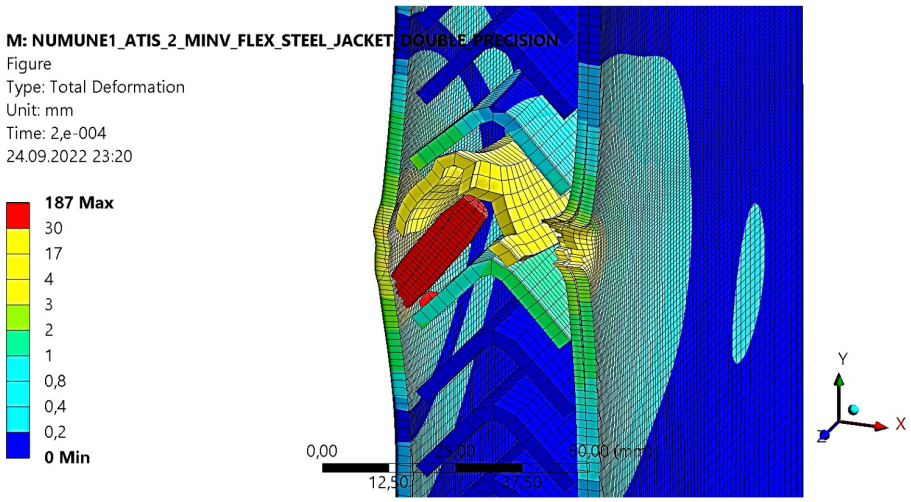

Figure 13 Deformation results of simulation below ballistic limit velocity in sectional view (Shot 2: 631 m/s).

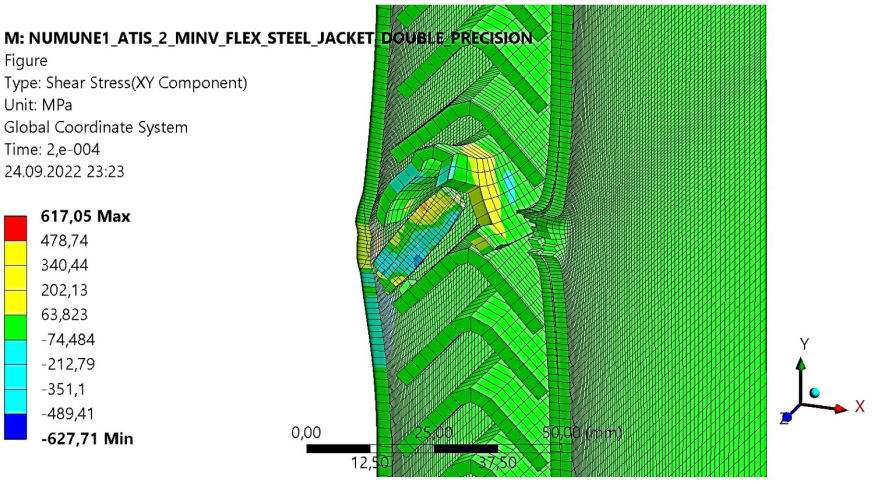

Figure 14 Shear stress distribution for Shot 2 in sectional view.

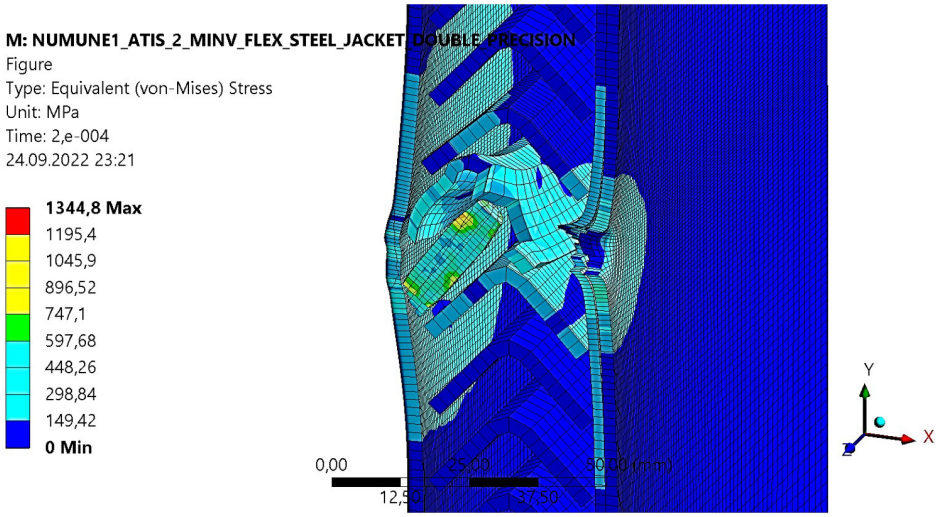

Figure 15 Von Mises equivalent stress distribution for Shot 2 in sectional view.

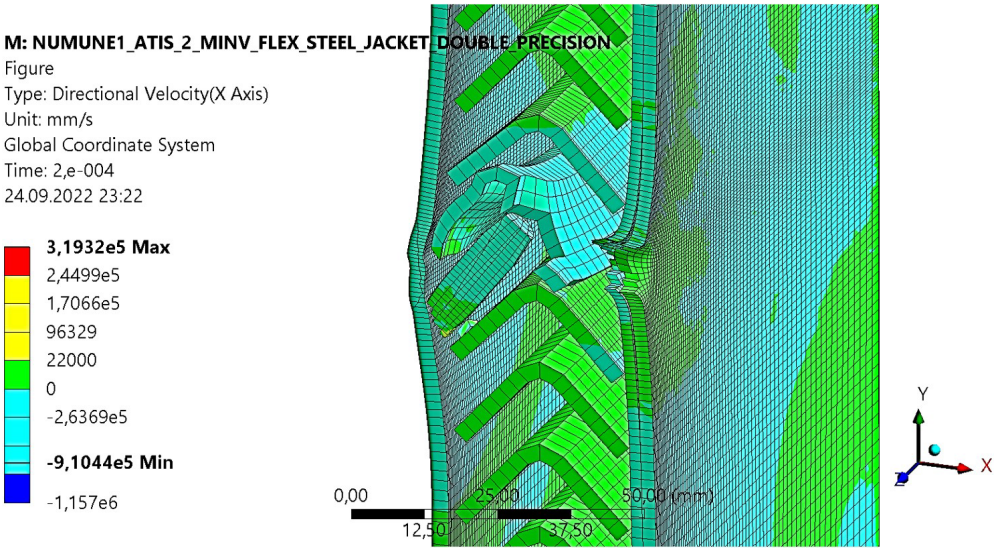

Figure 16 Velocity distribution for Shot 2 in sectional view.

Various ballistic scenarios simulated for Shot 1 (868 m/s) and Shot 2 (631 m/s). The results are shown in Figures 9–16. As can be seen from these figures, in Shot 1, the target was destroyed by a shot from 10 m (Figure 9); however, in Shot 2, the target blocked the passage of the projectile (Figure 14). The shear stress distributions (for both Shot 1 and Shot 2) are shown in Figures 10 and 14, respectively. The von Mises equivalent stress distribution is shown in Figures 11 and Figure 15. The initial linear portions of the curves represent the elastic-strain region. The following sections describe the regions where the target plastic deformed. The velocity distributions for Shot 1 and Shot 2 are shown in Figures 12 and 16, respectively. It was observed that the velocity remained constant after the initial rapid acceleration of the projectile. In the diagram series from Figure 17 to Figure 24, the time-dependent variation of the stress, deformation and velocity results mentioned above is presented. The data presented in these charts are the maximum and minimum values obtained over the entire model.

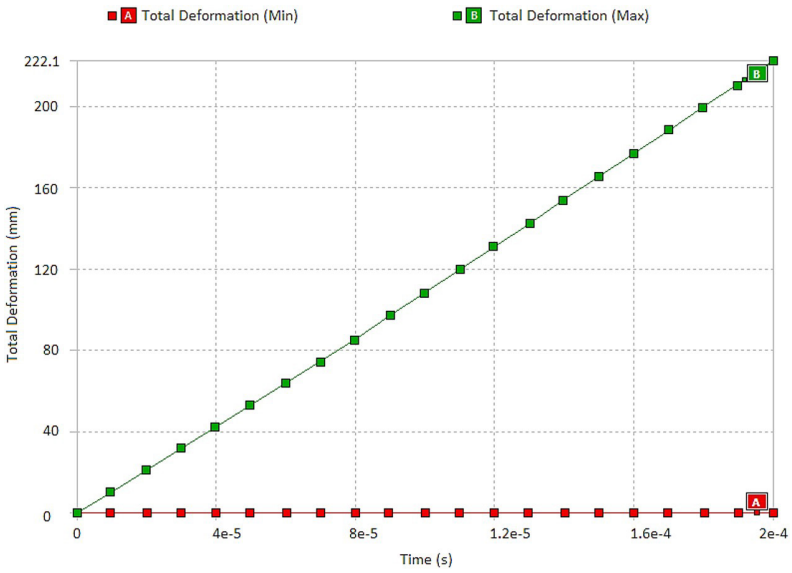

Figure 17 Time-dependent variation of deformation results of simulation ballistic above limit velocity (Shot 1: 868 m/s).

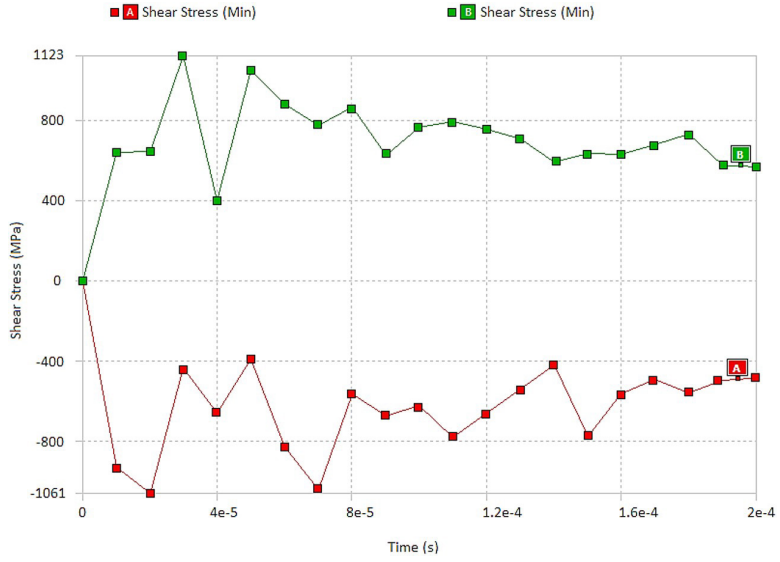

Figure 18 Time-dependent variation of shear stress results for Shot 1.

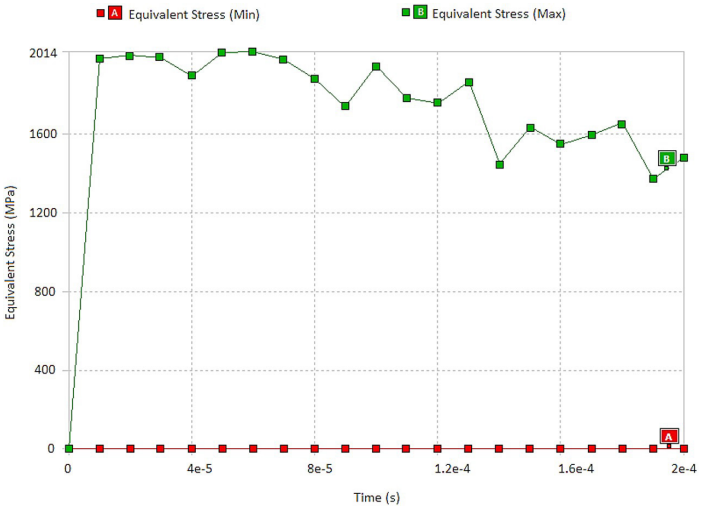

Figure 19 Time-dependent variation of Von Mises equivalent stress results for Shot 1.

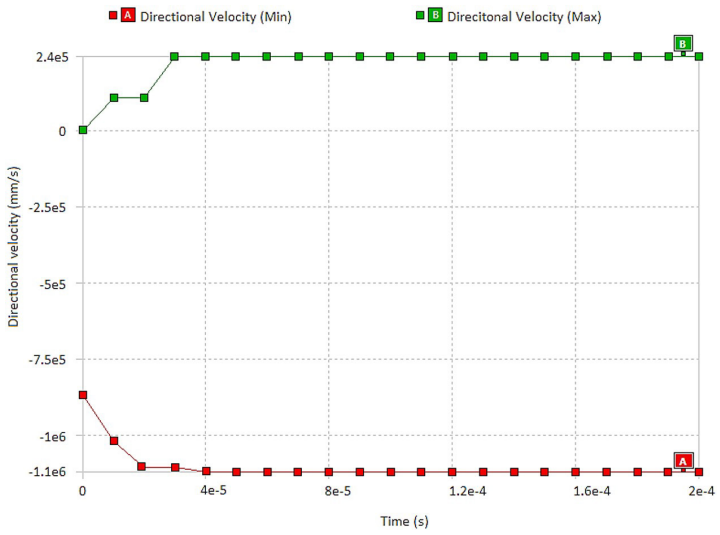

Figure 20 Time-dependent variation of velocity results for Shot 1.

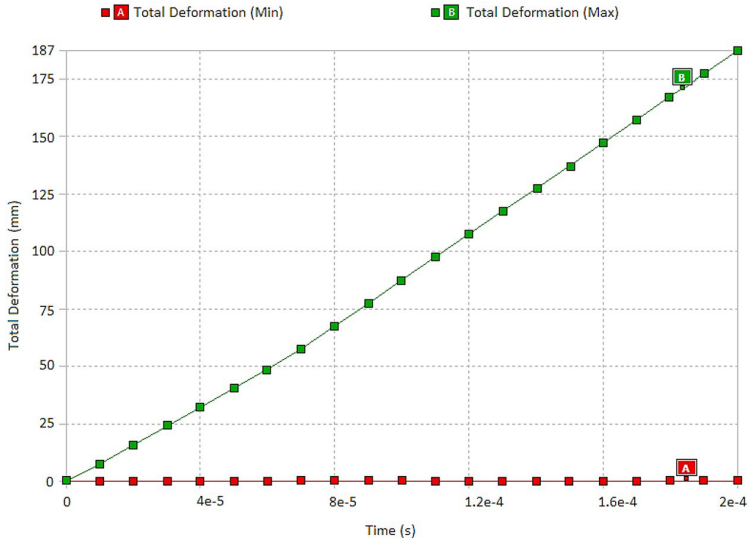

Figure 21 Time-dependent variation of deformation results of simulation below ballistic limit velocity (Shot 2: 631 m/s).

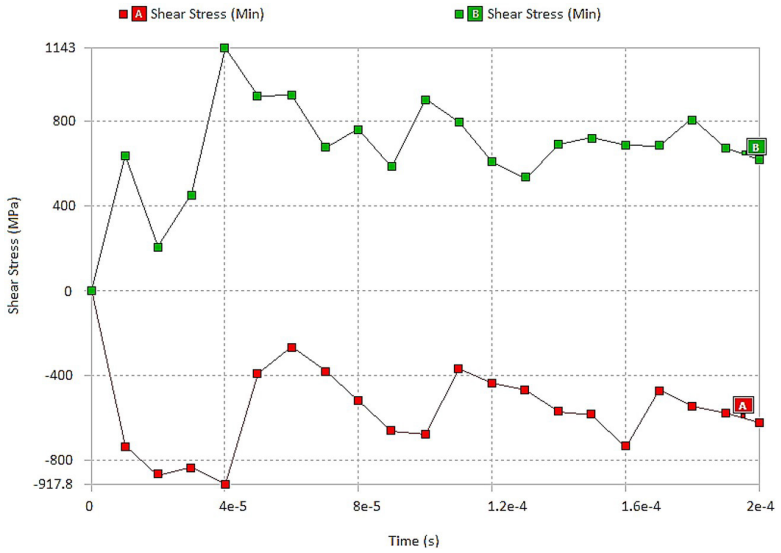

Figure 22 Time-dependent variation of shear stress results for Shot 2.

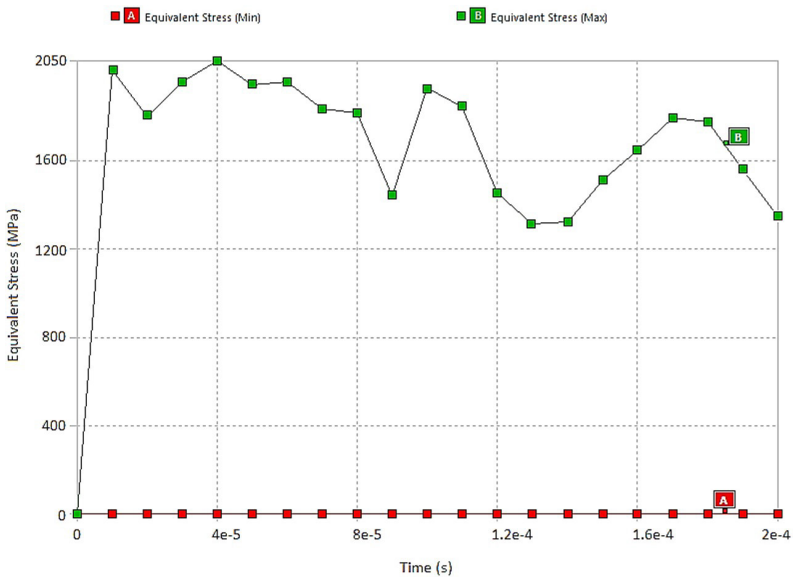

Figure 23 Time-dependent variation of Von Mises equivalent stress results for Shot 2.

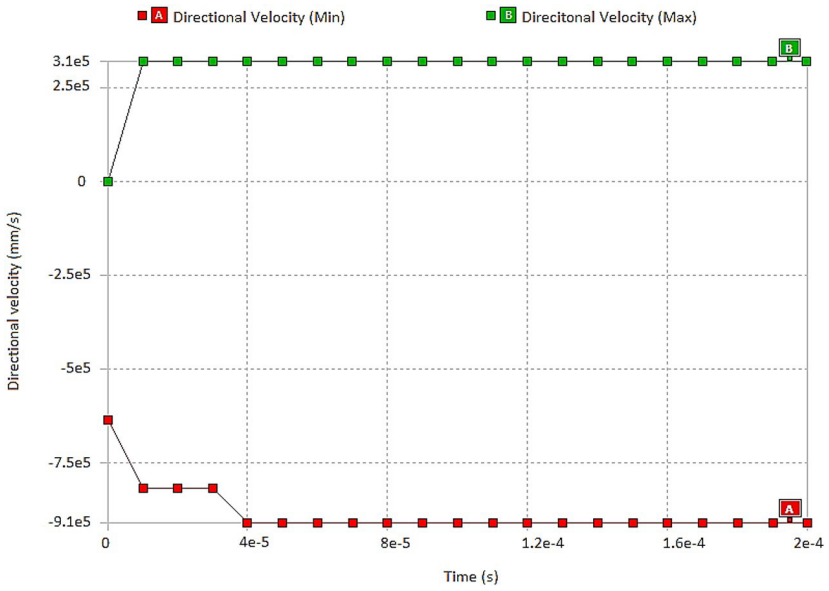

Figure 24 Time-dependent variation of velocity results for Shot 2.

3.2 Comparison between FEA and experimental results

Comparisons at the approximate scale are presented in Figures 25–30. Figure 25 shows the bullet exit side of the aluminum plate. Here, it is observed that for Shot 1, a bullet fired at a speed of 868 m/s penetrates the target. According to the images, it can be concluded that the experimental and numerical results of damage formation are in agreement. Figure 26 and Figure 27 show the bullet exit and entry sides of the deflector inner plates. Here, because the steel plates were bent in a V-shape, the forward direction of the projectile was deflected, thereby reducing the rate of advance. As can be seen, the numerical and experimental results were in good agreement. Figure 28 shows the rear steel sheet bullet exit side, and it is observed that the experimental and numerical results are similar.

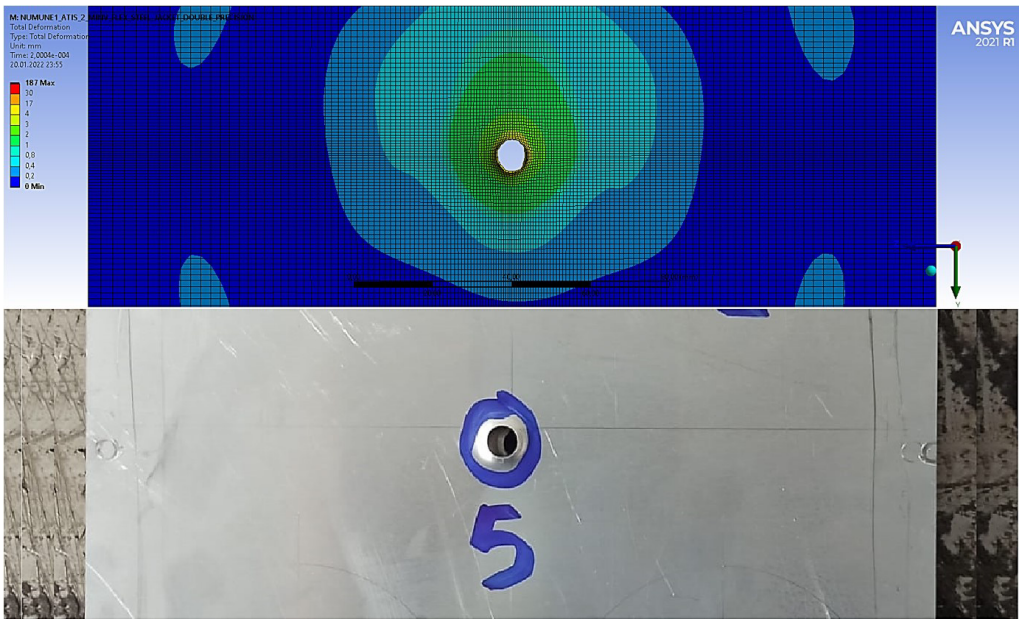

Figure 25 Bullet exit side of aluminum plate.

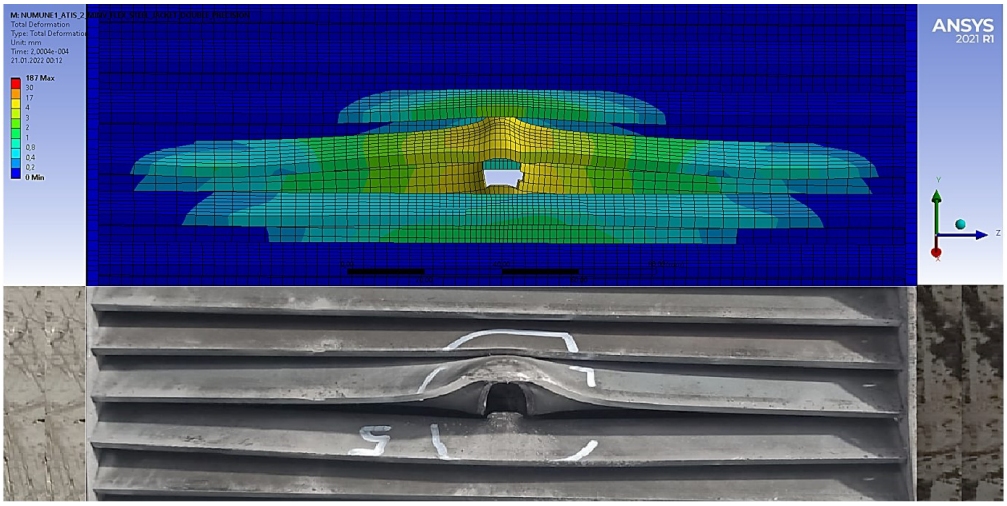

Figure 26 Bullet exit side of deflector inner plate.

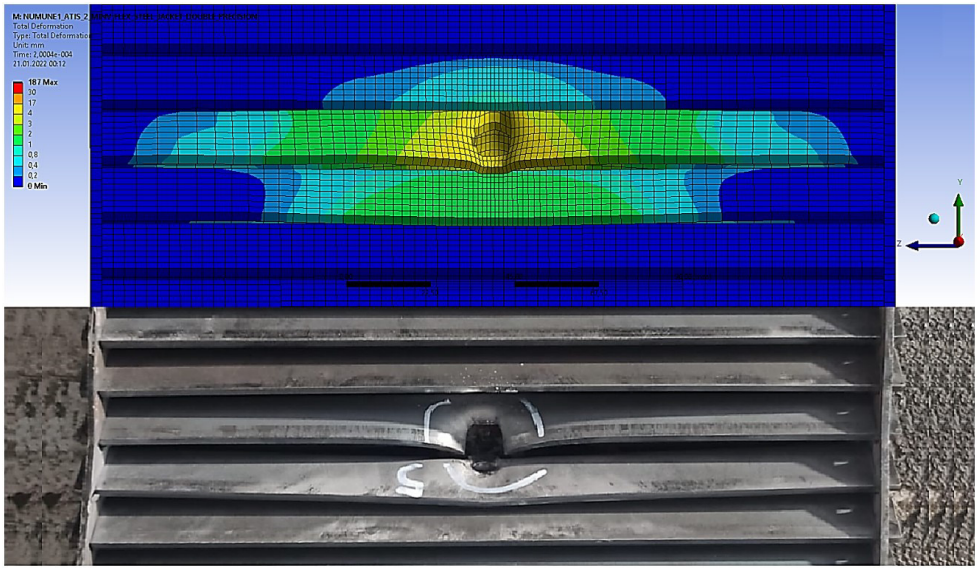

Figure 27 Bullet entry side of deflector inner plate.

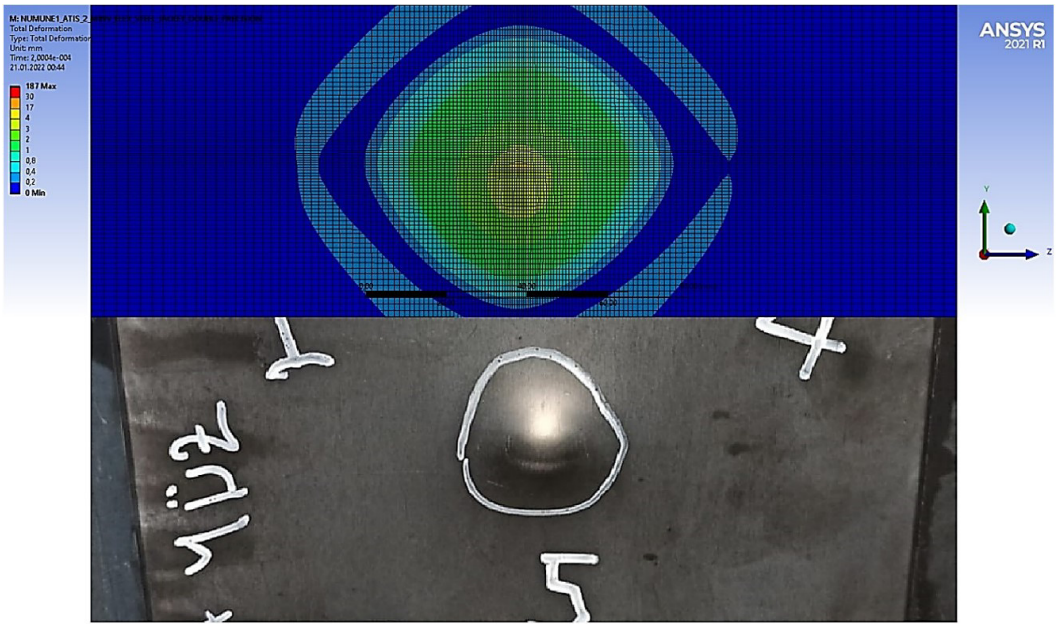

Figure 28 Bullet exit side of rear sheet steel.

Figures 29 and 30 show the experimental and numerical results of the deformations in the projectile impact zone and in the direction of the projectile motion. The numerical results were obtained at the maximum and minimum test speeds, but no tests were performed at intermediate speeds. A comparison of the numerical and experimental results in Figure 29 shows that the degree of deformation remains constant at about 7 mm. This is because the deformation of the Al-front plate remained constant at 7 mm, which may be because of the high ballistic velocity and small material wall thickness (2 mm) in Shot 1 (868 m/s) and Shot 2 (631 m/s). As shown in Figure 30, the deformations on the back plate decreased from 15 mm to 5 mm in numerical and experimental analyses. This may be because as the bullet first passes through the front plate, then the V-shaped steel plate, and finally the back plate, the velocity of the bullet gradually decreases, and a decreasing amount of deformation is detected in the back plate. In general, even with the current analysis results, the numerical analyses appear to be in agreement. The numerical results were obtained at the maximum and minimum test speeds, and no tests were performed at intermediate speeds. Therefore a first-order behavior is observed, the results of the numerical analysis are consistent. If a higher-order damage function is desired, interpolation values can be obtained with Taguchi-like approaches after the analyses at intermediate velocity values, and the results obtained from them can be added. The explosion protection performance of the structure protected with a single V-shaped plate was investigated in (Hafizi et al. 2017) and (Behera et al. 2021). In an earlier study (Panowicz et al. 2013), the protection of the V-shaped lower guard plate from land mines was investigated. However, the present study achieved the bullet-stopping performance by using a V-shaped pattern of plates. Thus, this study differs from other studies in the literature. In addition, the adiabatic shear formations mentioned in (Hazel 2016) and (İbiş 2021) are clearly observed in both shooting simulations.

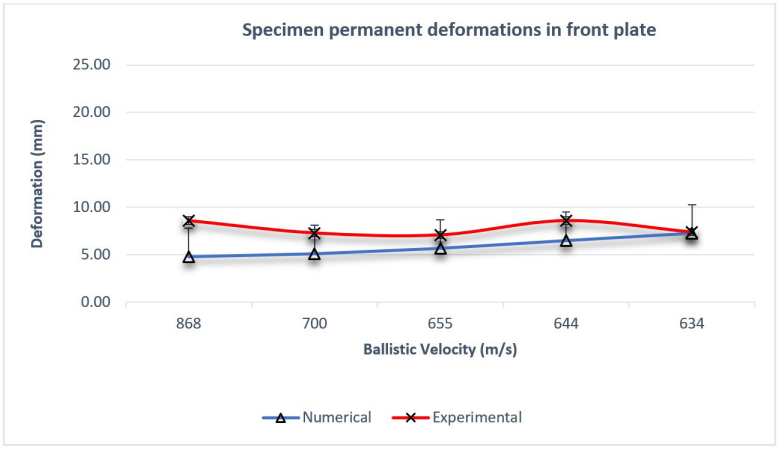

Figure 29 Numerical and experimental comparison of deformations on the front plate.

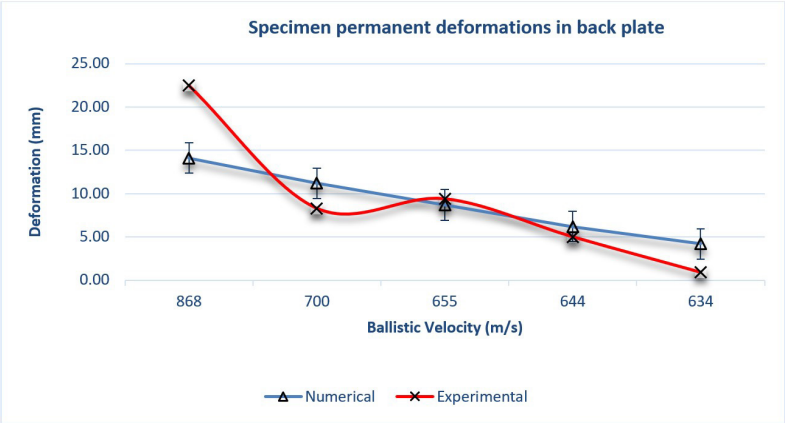

Figure 30 Numerical and experimental comparison of the deformations on the back plate.

4 CONCLUSIONS

The study and its results are summarized as follows:

a. In this study, the FE software ANSYS LS-DYNA was used for ballistic analysis. The J-C constitutive equation and damage model were used to model the behavior of metal armors under impact in ballistic scenarios. In addition to the J-C damage parameters, temperature-based damage was also defined in the simulations. The critical temperature value was taken as Tkr = 0.9Te.

b. The target plate was fired at from a distance of 10 m and at an angle of 90° to the steel plate bent in a V-shape between the aluminum plates at both ends. The effects of bullet velocity, plate thickness, and ballistic performance improvement techniques were analyzed both numerically and experimentally. After each impact, the penetration depth was measured, including the magnitude of plate bending in front of the target plate and bulging behind it.

c. In this study, samples with different combinations of different layers, such as aluminum–steel–aluminum, were created. Bullets with dimensions of 7.62 × 51 mm obtained from MKEK were used in the experiments. This study showed that different combinations of the same materials exhibit different ballistic behaviors.

d. In numerical simulation studies, the stress-strain curves for Al, steel, and bullet samples exhibited an elastic (linear) behavior in the initial period; subsequently, the stress increased with increasing plastic strain. In addition, it was observed that the stress showed a maximum value (1539 MPa) in the bullet, while the minimum value was obtained at St 37 (200 MPa). In addition, in the case of an increased deformation rate (1000/s), higher stress values were obtained owing to strain hardening.

e. In this study, until the stability of the model was verified, 16 simulations were performed, and two full models were determined as deformable-damaged and rigid bullet cores. With these models, a total of four simulations were carried out at the ballistic upper and lower limit velocities obtained in the experiments. In the 1st shot (speed of 868 m/s), the target was destroyed by a shot from 10 m, and in the 2nd shot (speed of 631 m/s), the target blocked the passage of the projectile.

f. A comparison of the FEA and experimental results showed that a bullet with a speed of 868 m/s in the 1st shot pierces the target. Here, it can be concluded that the experimental and numerical results of damage formation are in good agreement. Owing to the V-shaped bent steel plates inside the target, the forward motion of the projectile was deflected and the rate of advance was reduced. In this study, the numerical and experimental results were found to be in good agreement. Again, in the studies conducted for the rear steel sheet bullet exit side, it was determined that the experimental and numerical results were in good agreement.

g. In addition, experimental and numerical comparisons of the deformations in the projectile impact zone and in the direction of the projectile motion were performed. From a comparison of the numerical and experimental deformations of the front plate, it was observed that the degree of deformation remained constant at approximately 7 mm owing to the high ballistic velocity. From the measurement of the deformations of the back plate, the deformation decreased from 15 mm to 5 mm owing to the decreasing velocity of the bullet. In general, the experimental and FEA results were shown to be in good agreement.

Acknowledgements

This project was supported by the Research Fund of the Sakarya University of Applied Sciences (Project Number: 2021-01-05-035). We thank the Sakarya University of Applied Sciences for its financial support.

Author's Contribuitions: Investigation, M Çalışkan and E Camcı; Conceptualization, M Çalışkan and E Camcı; Methodology, M Çalışkan, E Camcı and F Findik; Software, M Çalışkan; Writing - original draft, M Çalışkan, E Camcı and F Findik; Writing - review & editing, M Çalışkan and F Fındık; Funding acquisition, M Çalışkan and F Fındık; Validation, M Çalışkan and E Camcı.

Editor: Marcílio Alves

References

Han, S.H., Hua, Z. (2011). Study on Blast-Resistant Structural Design of a Truck Cab. Applied Mechanics and Materials 66, 2136-2141, https://doi.org/10.4028/www.scientific.net/AMM.66-68.2136

M. N. Hafizi, Risby, M.S., Umar, S.T., Sohaimi, A.S.M., Khalis, S., Tan, K.S. (2017). Experimental and Numerical Investigation of V-Shape Plates Subjected To Blast Loadings. J. Fundam. Appl. Sci. 9(3S), 210-220, http://dx.doi.org/10.4314/jfas.v9i3s.18

Clayton, J.D. (2015). Modeling and Simulation of Ballistic Penetration of Ceramic-Polymer-Metal Layered Systems. Mathematical Problems in Engineering, Article ID 709498, https://doi.org/10.1155/2015/709498

Behera, S.K., Kumar, V., Kumar, A., Chawla, A. and Dubey, D. K. (2021). Numerical Modelling of V-Shaped Composite Plate Subjected to Blast Loading, Composit Materials for Extreme Loading. Proceedings of the Indo-Korean workshop on Multi-Functional Materials for Extreme Loading 495-504, Springer, Singapore, https://doi.org/10.1007/978-981-16-4138-1_32

Kang, H., Guo, X., Zhang, Q., Cui, H., Wang, S., Yan, W. (2021). Predicting the Behavior of Armored Plates Under Shallow-Buried Landmine Explosion Using İncomplete Scaling Models. International Journal of Impact Engineering 156 Elsevier, https://doi.org/10.1016/j.ijimpeng.2021.103970

Panowicz, R., Nowak, J., Konarzewski, M. (2013). Evaluation Of Impact Of The Deflector Shape On Effectiveness Of Weakening The Blast Wave Originating From A Mine Or Ied. Journal of KONES Powertrain and Transport, 20 (2).

D. Fernández-Fdz, R. Zaera, J. Fernández-Sáez (2011), A constitutive equation for ceramic materials used in lightweight armors, Computers and Structures 89 2316–2324 Elsevier, doi:10.1016/j.compstruc.2011.08.003

Christian C. Roth, Teresa Fras, Dirk Mohr, (2020), Dynamic perforation of lightweight armor: Temperature-dependent plasticity and fracture of aluminum 7020-T6, Mechanics of Materials 149 103537, Elsevier, https://doi.org/10.1016/j.mechmat.2020.103537

Qun Wang, Zhaohai Chen, Zhaofeng Chen (2013), Design and characteristics of hybrid composite armor subjected to projectile impact, Materials and Design 46 (2013) 634–639, elsevier, http://dx.doi.org/10.1016/j.matdes.2012.10.052

Kevin Doherty, Richard Squillacioti, Bryan Cheeseman, Brian Placzankis, and Denver Gallardy (2012), Expanding the availability of lightweight aluminum Alloy armor plate procured from detailed military specifications, 13th International Conference on Aluminum Alloys (ICAA13), TMS (The Minerals, Metals & Materials Society)

M. Grujicic, B. Pandurangan, U. Zecevic, K. L. Koudela and B. A. Cheeseman (2007), Ballistic performance of alumina/s-2 glassreinforced polymer-matrix composite hybrid lightweight armor against armor piercing (ap) and non-ap projectiles, Multidiscipline Modeling in Mat. and Str., Vol. 3, No. 3, pp. 287-312

M. L. Wilkins (1977), Use of Boron Compounds in Lightweight Armor, V. I. Matkovich (ed.), Boron and Refractory Boride, Section XIII © Springer-Verlag Berlin Heidelberg

Crouch, I.G. (2017). The Science of Armour Materials. Woodhead Publishing, Cambridge, https://doi.org/10.1016/B978-0-08-100704-4.00002-5

Zukas, J.A. (2004). Introduction to Hydrocodes, Elsevier, London.

Flores-Johnson, E.A., Saleh, M., Edwards, L. (2011). Ballistic performance of multi-layered metallic plates impacted by a 7.62-mm APM2 projectile. International Journal of Impact Engineering, 38 (12), 1022-1032, https://doi.org/10.1016/j.ijimpeng.2011.08.005

Borvik, T., Dey, S., Clausen, A.H. (2009). Perforation resistance of five different high strength steel plates subjected to small-arms projectiles. International Journal of Impact Engineering, 36, 948 964, https://doi.org/10.1016/j.ijimpeng.2008.12.003

CREO®8.0.1. (2021). Parametric Educational Edition, Parametric Technology Corporation, New York, USA.

Johnson, G.R., Cook, W. H. (1983). A constitutive model and data for metals subjected to large strains, high strain rates and high temperature. Proceedings 7th International Symposium on Ballistics, Lahey, 541-547.

Johnson Gordon R., Cook William H. (1985), Fracture characteristics of three metals subjected to various strains, strain rates, temperatures and pressures, Engineering Fracture Mechanics, Volume 21, Issue 1, 1985, Pages 31-48, Elsevier https://doi.org/10.1016/0013-7944(85)90052-9

Dehgolan, F.R., Behzadi, M., Sola, J.F. (2016). Obtaining Constants of Johnson-Cook Material Model Using a Combined Experimental, Numerical Simulation and Optimization Method. International Journal of Mechanical, Aerospace, Industrial, Mechatronic and Manufacturing Engineering 10(9).

Öztürk G. (2010). Numerical and Experimental Investigation of Perforation of St-37 Steel Plates by Oblique Impact, MSc Thesis in Mechanical Engineering, Middle East Technical University.

Hazel, P.J. (2016). Armor Materials, Theory and Design, CRC Press Taylor & Francis Group, 177-207.

İbiş, M.Ö. (2021). The Effect of Different Layers and Different Combination Techniques on Ballistic Performance in Armor Design, MSc Thesis, Sakarya University Institute of Science and Technology.

Garcia-Avila, M., Portanova, M., Rabiei, A. (2015). Ballistic performance of composite metal foams. Composite Structures, 125, 202-211, https://doi.org/10.1016/j.compstruct.2015.01.031

Fountzoulas, C.G., La Salvia, J. C. (2012). Improved modeling and simulation of the ballistic impact of tungsten-based penetrators on confined hot-pressed boron carbide targets. In: Swab JJ, Halbig M, Sanjaythur, editors. Adv. Ceram Armor VII. John Wiley & Sons, Inc.; 209–217.

Garcia-Avila, M., Portanova, M., Rabiei, A. (2014). Ballistic performance of a composite metal foam-ceramic armor system. Procedia Materials Science 4, 145 – 150, https://doi.org/10.1016/j.mspro.2014.07.571

ANSYS®R2021 (2021) Engineering Simulation Software, Ansys Corp. USA.